



HAL
open science

Vented gas explosion overpressure calculation based on a multi-layered neural network

Yann Gregoire, Jérôme Daubech, Christophe Proust, Emmanuel Leprette

► To cite this version:

Yann Gregoire, Jérôme Daubech, Christophe Proust, Emmanuel Leprette. Vented gas explosion overpressure calculation based on a multi-layered neural network. *Journal of Loss Prevention in the Process Industries*, 2022, 74, pp.104641. 10.1016/j.jlp.2021.104641 . ineris-03512902

HAL Id: ineris-03512902

<https://ineris.hal.science/ineris-03512902>

Submitted on 3 Feb 2022

HAL is a multi-disciplinary open access archive for the deposit and dissemination of scientific research documents, whether they are published or not. The documents may come from teaching and research institutions in France or abroad, or from public or private research centers.

L'archive ouverte pluridisciplinaire **HAL**, est destinée au dépôt et à la diffusion de documents scientifiques de niveau recherche, publiés ou non, émanant des établissements d'enseignement et de recherche français ou étrangers, des laboratoires publics ou privés.

Vented gas explosion overpressure calculation based on a multi-layered neural network

Yann Grégoire^a, Jérôme Daubech^a, Christophe Proust^{a,b}, Emmanuel Leprette^a

^a INERIS, PHDS dept., Parc Technologique ALATA, BP 2, 60550 Verneuil-en-Halatte, France

^b UTC, TIMR laboratory (EA4297), rue du Dr Schweitzer, 60200 Compiègne, France

E-mail: yann.gregoire@ineris.fr

Abstract

The case of a gas explosion occurring in a geometrically simple enclosure, equipped with a vent is considered. It is well known in the gas explosion scientific community that the calculation of the reduced explosion overpressure, determinant in safety studies, is not trivial. Not only there is a strong dependency on the chemical kinetics of the combustible but also on the enclosure geometry, the fluid flow, the vent mechanical behaviour, shape, etc... As a result, the modelling of the physics at stake is challenging, a wide range of models are proposed in the scientific literature and this reference situation is still the object of extensive research. A new simulation approach ignoring a large part of the underlying physics is investigated. It is based on the use of an artificial neural network (ANN). The focus is given on the method of use and results obtained with the ANN rather than on the neural network itself. Our observations are discussed within the scope of industrial safety problems. Calculations performed with the relatively simple ANN proposed in the official TensorFlow tutorial, on a vented explosion database containing 268 tests, led to surprisingly good results considering the ANN implementation efforts. The tool might look promising but is also far from being as trivial as it seems at a first glance: not only the results of simulations obtained with this type of model must be examined with the greatest care but also the initial data base must be very well controlled. Routes are proposed to enhance the initial database and perform relevant analyses of the neural network predictions.

Keywords: prevention, mitigation, industrial explosions, ...

1 Introduction

From automotive technologies to financial forecasting or climate modelling, AI based algorithms are progressively emerging practically in all scientific fields. They can provide quick estimations or classifications with an acceptable accuracy. Above all, they promise an extreme capability to perform regressions on practically any kind of data. Example can be found relatively easily on internet on neural networks-based algorithms that reproduce efficiently the structure and presentation of a given random text that can be either a Shakespeare's work or a mathematics book including figures (Karpathy, 2015). In that example the neural network can built grammatically correct sentences, in a text that makes no sense. More generally, such models rely on data interpretation that may have been obtained through calculations or experiments. In various applications, these calculation methods completed or even entirely replaced the complex mathematical models used before. Current works investigate the possibility for such models to provide estimations of the overpressures following a gas explosion in a vented enclosure. The physics of gas explosion venting involve tremendously complex phenomena, of flame propagation in fluid structure coupled problem in which not only the chemical reaction has an importance, but also the enclosure geometry, ignition location, vent characteristics, internal as well as external flow conditions, among others. In this paper, INERIS experimental data is used together with published experimental data (see references) gas explosions on (hydrogen, methane, ethylene and propane) in vented vessels to calibrate a multi-layered neural network. The TensorFlow library (Abadi et al., 2016) and its sub-library Keras are used to build and run the model. TensorFlow was released by Google under the Apache License 2.0 on November 9, 2015. The Keras library is barely older and was initially released on the 27th March 2015 by Chollet.

Our investigation on the neural network capabilities and performance is taken under the angle of a regression problem. Various parameters are used as input data, such as the type of gas, concentration, turbulent velocity u' before ignition, mixture expansion ratio, enclosure or vent dimensions. The selected data only consist in variables that depend on the test setup and can be accessed before conducting the explosion venting test in each configuration. The neural network is used to estimate the reduced explosion pressure. It is trained using older INERIS data test and/or published data. Then, it is confronted to other tests that:

- are not part of the training data,
- are performed on a vessel different from those listed in the training data.

The underlying idea is to examine if this tool that relies on a purely mathematic model, entirely ignoring the physics of gas explosion venting, can perform predictive calculations and under which conditions.

2 Neural network

2.1 Paradigm of supervised learning

As this work is dedicated to explosion science experts rather than neural network specialists, the paradigm of supervised learning with neural networks, which is used here, is briefly described. If not purely mathematical, the modelling of a physical phenomenon in the traditional approach consists in building a model from the physical understanding of the phenomenon then confronting it to a reference: an experimental or numerical observation. Obtaining a comprehensive generalisable model is the final purpose.

With artificial neural networks and supervised learning, the paradigm is changed as the model structure is chosen at the beginning and initiated partly randomly. It may consist in a large and complex structure of several interconnected functions and comprising a large number of adjustable coefficients. The network is fed with data D , and deliver a result R . Following this step, the model result is compared to the expected measurement M and the inner coefficients of the neural network are adjusted to minimize the error between R and M . Because it is a statistical approach, this inductive process is to be repeated several hundred or thousands of times ideally on a large dataset to obtain the best possible fit. This process is called the training or learning phase. At the end of the learning process, the model is not directly interpretable and despite all the inner structure of the neural network is accessible, it may be seen as a black box from a physicist point of view. To use it, a new sample of data with the same format at that used for the training phase, is fed to the network, which gives a new result. This is called the prediction phase.

2.2 Structure and function of the MLP

In the current study, a specific type of artificial neural network (ANN) is used referred as “multilayer perceptron” (MLP) to estimate the overpressure obtained during a confined gas explosion in a vented enclosure. It consists in several densely connected layers of artificial neurons converging to a single output. This neural network architecture is chosen as it is particularly well suited for regression problems (Cybenko, 1989). Analogies can be made between artificial neural networks functioning and the behaviour of neurons in a brain. In the present context, the neurons can be considered as mathematical functions that maps a given input to a desired output. An example is given in the next figure:

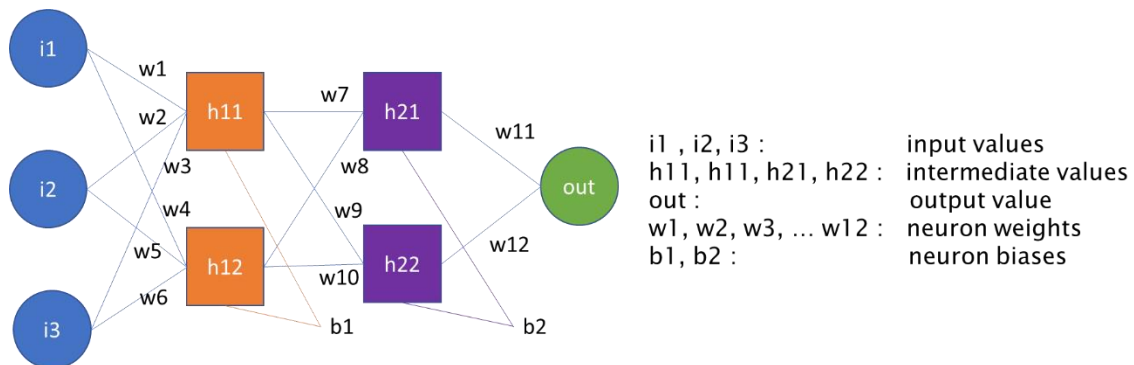


Fig. 1. Schematic of a 3 layers MLP network, with 3 input features and a single output

Thus, the first step is to select the network architecture: that is the numbers of layers and neurons in each layer. This is unfortunately entirely empirical. Despite some specific architecture have been identified to function well in certain cases, there is absolutely no rule to dimension the neural network, except possibly a very general recommendation to build a network as small as possible for a given task.

Then in such network, an activation function σ is selected, in most cases, it is a continuous (derivable) functions yielding outputs between 0 and 1 or -1 and 1. A famous one is the sigmoid function:

$$\sigma(z) = \frac{1}{1+e^{-z}} \quad (1)$$

To use the neural network, it must firstly be trained, to set its internal weights (w_i) and biases (b_i). This is performed through a feedforward, loss estimation and back propagation phase. To put it simply, the user needs to know the real output for a given set of inputs. This first set of information is referred as the training data.

In the current example, the input features are the conditions in which a given experimental test is performed and the “real output” is the P_{red} obtained. Then the input features values are passed through the network, and an output estimation is obtained. For a single test, with the scheme of *Fig. 1*, this operation takes the form:

$$\begin{cases} h_{11} = \sigma(i_1 \cdot w_1 + i_2 \cdot w_2 + i_3 \cdot w_3 + b_1) \\ h_{12} = \sigma(i_1 \cdot w_4 + i_2 \cdot w_5 + i_3 \cdot w_6 + b_1) \\ h_{21} = \sigma(h_{11} \cdot w_7 + h_{12} \cdot w_8 + b_2) \\ h_{22} = \sigma(h_{11} \cdot w_9 + h_{12} \cdot w_{10} + b_2) \\ out = \sigma(h_{21} \cdot w_{11} + h_{22} \cdot w_{12}) \end{cases} \quad (2)$$

The “out” value is the first estimated P_{red} , that will be noted $\overline{P_{red}}$ to avoid confusion with the real value. The feedforward propagation phase is performed for the complete dataset, to obtain a range of estimations of P_{red} . Then the “correctness” of the estimation is examined using a loss function, which in our case consists in the mean square error (mse) evaluation (note that other loss functions such as mean absolute error or custom models may also be used).

$$mse = \sum_{all\ tests} (\overline{P_{red}} - P_{red})^2 \quad (3)$$

At last a backpropagation phase is performed to update the weight and biases of the neurons in view of reducing the error. This is the most complex part as in consists in calculating for each weight the partial derivative of the loss function. Details of this calculation may be found in the scientific literature. The important information here is that each weight is updated following a learning rate η , in view of minimizing the final error - the ‘mse’ in our case.

In the field of artificial neural network, a cycle of processing through the complete dataset is referred as an “epoch”. Several dozens of epochs may be needed to train the neural network. Note that the initial weights are set randomly in the codes, so that if the user does not alter this initial random distribution, running the same training twice should give close but different results.

Once calibrated with the training data, predictions can be made on the “test data”: a set of data that passes only through the feedforward propagation phase, with no updating of the weights. In practice the prediction phase is used on 2 occasions:

- 1) In our case, to perform estimations of the P_{red} for given test configurations that are not part of the training dataset. If the experimental measurement is not known, this estimation can be referred as a prediction of the neural network.
- 2) The second case of use of the prediction method is actually part of the training process. In practice at each epoch, the algorithm selects a certain percentage of the training data (80 %) to perform the learning tasks then runs a prediction phase on the unused data. The resulting error is named “validation error” and is different from the error calculated on the used data, referred as “loss”. Thus, in the current work we have at each epoch a validation set of data that is not part of the data used for training nor of the test data (used after the learning phase to make the predictions). Comparison of the evolution of both errors is helpful to examine the convergence of the neural network and eventually stop the training earlier if no progress is made on the validation set. It is also helpful to detect when the model is overfitted. Schematically overfitting could be seen as a model that passes through every point but fails at extracting the general trend, while the underfitting would be the average of the solution vector:

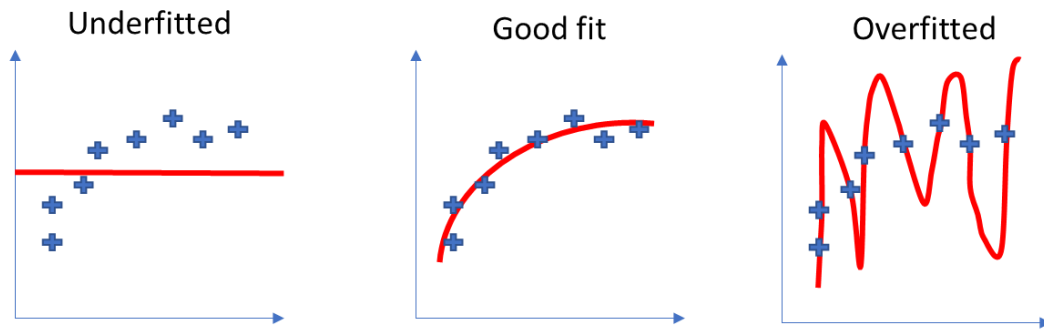


Fig. 2. Illustration of model underfitting or overfitting

2.3 A practical example

An example on the TensorFlow official website in date of March 2021, considers the examination of the fuel efficiency of various motors as function of 8 of their characteristics, made of numeric data such as the motors weight and textual data such as the origin of fabrication. After a proper transformation of the textual data into 3 categories for the 3 possible origins of the motors in the database, the training set consists in 398 lines (named instances) over 10 input columns (named features) and a single column of results (containing a value for fuel efficiency). The selected neural network to solve this problem comprises two layers of 64 neurons, leading to 4865 trainable parameters. With 398 instances and 1000 epochs, the number of operations is considerable. Even so, the now popular AI frameworks such as TensorFlow and Keras used here, were developed in view of drastically simplifying the implementation and efficiency of such algorithm. The complete coding of such solution in Python is a matter of less than a hundred of lines of code, and the algorithm runs within a few minutes on a standard CPU. Using specific software such as Orange3 (Demsar et al., 2013) allows to perform the same tasks through visual programming, practically without entering any line of code.

2.4 Selected solution

Present work does not aim at looking for the best network architecture but is focused on the use of such tool and the changes it might bring to our field of experience. For this reason, a single MLP is used for the whole study. Starting from the example proposed on TensorFlow website applied to our data, a limited number of tests was performed using various parameters for the network architecture and functions in the early steps of this study to select our best candidate. It relies on 4 densely connected layers of 32 neurons each, for a single output. The chosen activation function is the 'ReLU' function, with the 'Adam' optimizer and the mean square error loss function. These are also the same functions as those used in the example of the official TensorFlow website. A schematic of the MLP structure is presented in Figure 3 (deeper details on the input and output of the MLP are given in the subsequent paragraphs):

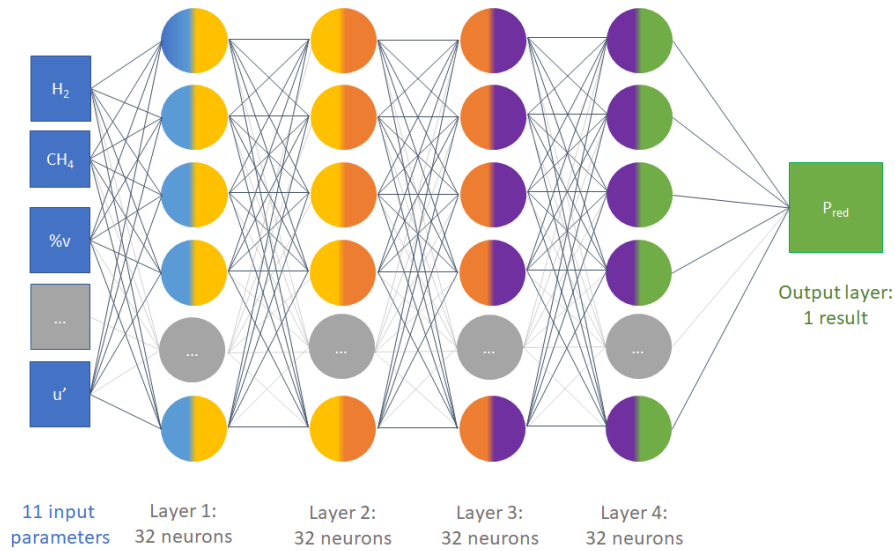


Fig. 3. Schematic of the MLP structure used in this study

3 Experimental data

3.1 Phenomenon studied

The reference case of interest is a vented gas deflagration. The situation is that of an explosible gas mixture ignited in an enclosure equipped with an opening referred as a “vent”. The pressure growth in the enclosure eventually leads to the vent opening and discharge of the gases to the surrounding atmosphere with a possible external explosion. Vented deflagrations have been studied since the 1950th. The physics is not yet totally clear, and the modelling remains challenging. Cooper et al. (1986) published a rather detailed analysis of the explosion dynamics and identified several successive pressure peaks and complex signal shapes, that depend on the explosion conditions.. A typical experimental signal recorded during such event is presented in Fig. 4.

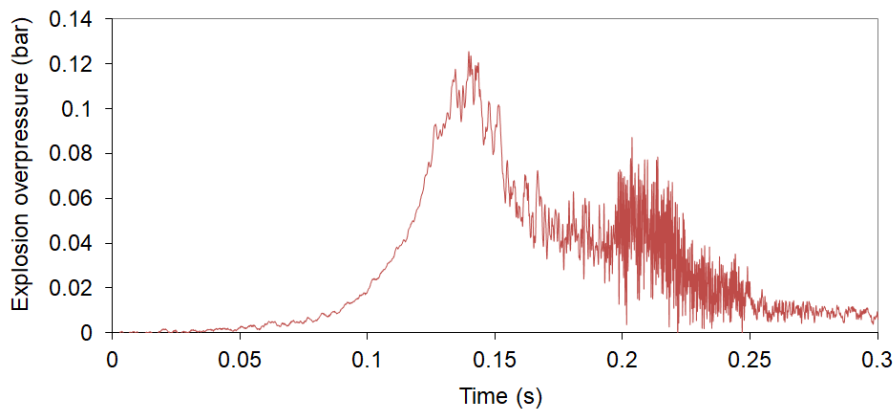


Fig. 4. Example of experimental signal of the overpressure recorded during a vented gas deflagration (16.5 % H₂-air ignited at the center of a 4 m³ vessel with a 0.5 m² vent)

The relative importance of the local maxima visible in Fig. 4 or the acoustic perturbations starting after $t = 250$ ms are common features described by Cooper et al. (1986), they depend on the test parameters, among which the nature and concentration of the combustible gas, the ignition location and the vessel and vent geometries. At the same period of time, no venting model was able to account for all this phenomenology. Here we are only interested in the maximum value of the overpressure measured during the explosion, referred as P_{red} .

3.2 Raw data

Data concerning vented gas explosion was extracted from Bauwens et al. (2011 ; 2012a and 2014) ; Chao et al. (2011) ; Daubech J. et al. (2011) ; Fakandu et al. (2013) ; Kumar et al. (1989 ; 2006 and 2009) ; Liang (2017) ; Pasman et al. (1974) ; Skjold et al. (2019) ; Sun et al. (2018) ; Wang et al. (2018) and Yao C. (1974). Note that the works from Daubech et al. (2011) consists in tests performed by the authors of the current paper. In total we found 202 published tests. Other still unpublished data from INERIS is used hereafter, which consist in 90 tests. Because printing all those tests in the current paper would be unpractical (268 lines over 17 columns) and is not necessary for the current analysis, only a sample is presented as an illustration in tables 1 and 2 thereafter. Geometric data on the test vessel (shape, volume, vent area, vent bursting pressure), information on the fuel (nature, concentration, laminar burning velocity, expansion ratio) are listed with the maximum recorded overpressure.

Table 1: Randomly selected lines in the database, left side columns. *L*, *W* and *H* respectively stand for the length, width and height of the rectangular enclosures (for cylinders, *L* is for the length, but *W* and *H* are both the vessel diameter; for spheres, only the diameter is displayed)

Test #	Author	Year	Fuel	%vol	L (m)	W (m)	H (m)
2	Bauwens	2011	Hydrogen	16.5	4.6	4.6	3
49	Chao	2010	Hydrogen	18	4.6	4.6	3
69	Daubech	2011	Hydrogen	14	5.5	1.6	1.6
102	Kumar	1989	Hydrogen	10	2.36	2.36	2.36
118	Kumar	2009	Hydrogen	5.9	10	4	3
155	Liang	2017	Hydrogen	6.2	4.5	4	3
171	Skjold	2018	Hydrogen	15	5.867	2.352	2.385
177	Sun	2018	Ethylene	7	2	1.2	0.6
197	Wang	2018	Hydrogen	34	1.8	1	0.55
218	Ineris	2019	Hydrogen	10	2	1	2
266	Ineris	2009	Methane	11.1	1.83	0.834	0.834

Table 2: Randomly selected lines in the database, right side columns for the same tests as in Table1 – The shape column refers to the vessel volume, shape, the ignition is performed either at the amrous of the vessel or at its back (BW stands for backwards) far from the vent u' is the turbulent velocity at ignition time

Test #	V (m ³)	Shape	Av (m ²)	Ignition	P _{stat} (bar)	u' (m/s)	P _{red} (bar)
2	63.7	Rectangle	5.4	Centre	0.005	0.1	0.03
49	63.7	Rectangle	2.7	Centre	0.005	0.1	0.234
69	10.5	Cylinder	2	BW	0.005	0	0.03
102	6.85	Sphere	0.0491	Centre	0.1	0	0.9
118	120	Rectangle	0.55	Centre	0.005	1	0.1
155	57	Rectangle	0.55	Centre	0.01	1	0.05
171	33	Rectangle	5.56	BW	0.005	0	0.03
177	1.44	Rectangle	0.18	BW	0.075	0	0.13
197	1	Rectangle	0.2	Centre	0.005	0	0.95
218	4	Rectangle	0.49	BW	0.005	2.2	0.36
266	1	Cylinder	0.042	Centre	0.1	1.5	1.37

All information listed in this table, except P_{red} is known before the test. We intend to use this information in a neural network to predict P_{red}. In total, the database contains test results:

- from 22 different studies from 12 authors between 1974 and 2019,
- of tests performed in 18 different volumes:
 - ranging from 10 l to 120 m³,
 - of parallelepipedal, cylindrical or spherical shapes,
 - with vents of static opening pressure P_{stat} up to 300 mbar but with a vast majority (259 over 268) under 100 mbar, including 200 tests with P_{stat} under 20 mbar.
- performed mostly with hydrogen (180) and methane (60), but also including propane (9) and ethylene tests (19),
- mostly in fluids at rest as 185 tests over 168 were performed with a turbulent velocity u' lower than 0.1 m/s
- with P_{red} recorded up to 2 bar but almost 60 % of the tests in the 0-200 mbar range (and 90% of tests below 1 bar).

If the data is grouped by study (author and year), by fuel and by vessel volume, 30 “independent” sets of data can be formed.

Several of these tests were performed in the scope of studying the effect of low P_{stat}, inertia-less vent panels that often consisted in plastic foils glued to the vessel, attached with duct tape or held with low strength magnets. As such, the P_{stat} is not a calibrated value and should rather be seen as an estimation based on experimental observation. However, an order of magnitude is enough here, as the purpose of current work is the examination of the neural network, rather than an optimal description of the physics of the explosions.

3.3 Data formatting

A first issue arises for the physicist here: which data would be relevant to solve this problem? The authors of the current paper are specialists of industrial explosions. Other profiles may select other data, possibly not relevant to the problem. As this work targets to experts in explosion, we will not expand more on this aspect. It is however important to remind that the works considered here depend on this selection of relevant parameters. For instance, we will not rely on the laminar flame velocity and burnt gas expansion ratio (which

could however be an option), but only on the gas nature and its volume fraction - which are related to the former parameters.

Then, there is an issue with the format of the data: how to differentiate in the neural network whether hydrogen or methane is tested, or the difference between central and backward ignition.

To overcome difficulties related to the gas nature, it has been decided to categorize the type of gas and replace the gas name column with 4 columns: "hydrogen", "methane", "propane" and "ethylene", that contains a value of 1 or 0 depending on the gas considered. As published on TensorFlow official website, this appear to be a common practice in neural network related problems.

To account for the dimensions and shape factor of the enclosure, it has been decided to retain the vessel hydraulic diameter, its length and volume and consider a shape variable equal to 0 for cuboids, 1 for cylinders and 2 for spheres.

Then, to model central or backward ignition, we simply use the distance from ignition point to the vent.

As a result, a 268 lines table containing only numbers over 11 columns is obtained. The columns correspond respectively to the type of gas (4 columns), gas volumetric concentration in air, vessel shape coefficient, length, diameter and volume, the ignition location coefficient, the vent area and its static opening pressure, the turbulent flow velocity u' at ignition, and finally the P_{red} measured in the test.

Note that the P_{red} is the result vector and all columns before that, correspond to data that are directly part of the test configuration and no specific modelling such as flame velocity calculation is considered.

The principle here is to train the ANN on this test data in the so-called training phase. Then in the prediction phase, the knowledge of P_{red} is required. In other words, once the training is terminated, the knowledge of the test parameters is enough with no further calculation of any intermediate variable, to estimate a P_{red} .

3.4 Data splitting

The goal of the present study is not the development of a code able to predict the vented vessel overpressure in case of a gas explosion, but to examine the capabilities of the neural network to do so. Therefore, several tests are designed in view of examining the performances and robustness of the neural network. They consist in using a part of the data to train the network, then validate it with the other part, that has not been used for the training. It is the same work as that performed during the training, with the difference that the data used later for validation is chosen by the user rather than randomly selected by the code. Two types of data splitting are investigated: the general random separation and the laboratory or group separation.

3.4.1 Basic configuration: general random data separation

In this case, 10 % of the tests are randomly selected as test data in the original 268 test table. During a same study, the tests configurations can be assumed to be relatively similar because the vessel and fuel are the same, in some occurrences only the fuel concentration is varied. Removing a few samples for the database and trying to test the missing configurations should yield satisfying results. The subjacent idea is that if knowledge of the test results in similar conditions is available, the network should perform well.

3.4.2 Laboratory/Group data separation

Here, the separation is between our (INERIS) measurements and the other published. The question concerns the generalisation capabilities of the model: can we, from our tests only, predict all the results published by other scientists on this topic? and the opposite: would it possible to find the INERIS measurements from the data published by researcher other than those from INERIS? This approach differs from the earlier as, in this case, the test configuration may differ significantly between the test and the training data. For instance, INERIS has neither 63.7 nor 120 m³ vessels.

Then other tests are performed selecting randomly 3 groups of studies as test data. The 30 groups available in total correspond to tests from different studies/publications also with different fuels and different vessels.

3.5 Data augmentation

Each time a training data set is prepared from the earlier separation, it is expanded through a data augmentation method. Neural networks are particularly efficient when large amounts of data are available, while they tend to lack of stability with smaller data samples. However real scale explosion tests involve

significant costs, and their number is limited. Given the fact that we need to reduce our database to perform the validation tasks, the number of tests becomes insufficient. Based on the idea that experimental measurements may not be exact, the dataset is expanded 100 times supposing for each relevant feature (typically not the gas nature) a random error factor between 0 and a maximum. This maximum is 5 % for the metric dimensions: those of the vessel, the vent, the ignition location. An error up to 5 % is also assumed on the vent P_{stat} and the measured P_{red} , while a maximal error of 1 % is considered on the fuel volume fraction. To put it simply, for a test with 10 % of methane gas, the algorithm generates 100 neighbours with a random methane concentration between 9.9 and 10.1 %. Different random factors, within the ranges described earlier, will also be applied simultaneously to the other variables of the same test.

3.6 Data and code publication

In paragraph 2.3, it has been asserted that the data manipulation and development and use of MLP based method with libraries such as TensorFlow in Python is relatively accessible, without significant knowledge in computer sciences. To illustrate this point, the code used to prepare the current article is published on a Zenodo repository (Grégoire, 2021, <https://doi.org/10.5281/zenodo.5497942>). It consists in 2 csv files containing the test database and the rules used to perform the data augmentation, as well as 3 python files dedicated to the data augmentation algorithm, the construction, training and use of the MLP. The example given in the repository concerns more specifically the works discussed in paragraph 5.1: the random selection of 10% of the tests in the database as independent test data, the 90 % other being the data firstly augmented then used to train the network. However, enough material is given to be able to reproduce all of the MLP results shown in the paper, as the user will only need to tweak either the selection in the original database (most cases) or the creation (for physical tests) of the test data.

4 “Traditional” modelling approach

In view of comforting the analysis, a few of the ANN predictions are also compared to those made with various kinds of empirical or phenomenological model. However, the purpose of this section is not to document the model performances but rather to highlight the complexity of the phenomenon described and give a focus on the consequent research work still needed.

4.1 Bartknecht model and NFPA 68:2013 model

A first basis of comparison is the Bartknecht formulas that is used in the EN 14994 (2007) standard on gas explosion venting. It takes the form

$$A_v = \{[0.1265 \log_{10}(K_G) - 0.0567] \cdot P_{red}^{-0.5817} + [0.1754 \cdot P_{red}^{-0.5722}(P_{stat} - 0.1)]\} \cdot V^{2/3} \quad (6)$$

With A_v the vent area, K_G the gas explosion index, P_{stat} the vent static opening pressure and V the enclosure volume.

This formula is generally admitted being overly conservative except in the case of turbulent deflagrations of highly reactive gases (such as hydrogen).

Alternatively, the National Fire Protection Association’s (NFPA) standard on Explosion protection by deflagration venting, NFPA 68, provides venting models for gaseous mixtures explosions. This standard is regularly updated, and the model can change drastically from one release to the next. Here the example of the 2013 version is presented. The expressions are presented in such a way that the vent area A_v can be calculated as function of the reduced internal overpressure P_{red} .

If the reduced overpressure P_{red} is lower than 0.5 bar :

$$A_{v,0} = \frac{S_u \rho_u \lambda}{2 G_u c_d} \left[\left(\frac{P_{max} + 1}{P_0 + 1} \right)^{\frac{1}{\gamma_b}} - 1 \right] (P_0 + 1)^{\frac{1}{2}} \cdot \frac{A_s}{P_{red}^{1/2}} \quad (7)$$

When the reduced overpressure P_{red} is over 0.5 bar :

$$A_v = A_s \frac{\left[1 - \left(\frac{P_{red}+1}{P_{max}+1} \right)^{\frac{1}{\gamma_b}} \right]}{\left[\left(\frac{P_{red}+1}{P_{max}+1} \right)^{\frac{1}{\gamma_b}} - \left(\frac{P_{stat}+1}{P_0+1} \right)^{\frac{1}{\gamma_b-1}} \right]} \frac{S_u \rho_u \lambda}{2 G_u C_d} \quad (8)$$

Where

- A_s is the internal area of the enclosure
- P_{max} is the maximum pressure developed in a closed deflagration by ignition of the same flammable mixture (in bar)
- P_0 is the enclosure pressure before the ignition (in bar)
- S_u is the laminar burning velocity of the flammable mixture
- ρ_u is the density of the unburned flammable mixture
- G_u is the unburned flammable mixture sonic flow mass flux ($G_u = 230.1 \text{ kg/m}^2 \cdot \text{sec}$)
- λ is the flame wrinkling factor due to the turbulence and flame instabilities
- γ_b is the ratio of the specific heats for the burned gases (between 1.1 and 1.2 depending on the gas mixture)
- C_d is the vent flow discharge ($C_d = 0.8$)
- P_{stat} is the nominal vent deployment or the static activation pressure (in bar)

The flame wrinkling factor λ calculation is not trivial, it depends on various parameters such as the presence of obstacles and the Reynolds number at the vent.

Rodgers et Zalosh (2013) showed that NFPA68:2013 model gave conservative estimations of the vent area in a vast majority of industrial cases. Fakandu et al (2013) compared both NFPA68:2013 and EN14994:2007 models and demonstrated a better fit on experimental data with the former, despite it seem insufficient in cases with turbulent hydrogen, or when many small obstacles are present near the vent.

4.2 Ulster University models (Molkov, 1999 - 2014)

Molkov et al. (1999) proposed a model considering the flame instabilities and of the interaction between flow created by the vent (turbulence) and the internal explosion. These two aspects are covered using the laminar and turbulent "Bradley" numbers (Br and Br_t : Bradley and Mitcheson; 1978). The turbulent Bradley number depends on the Degree Of Interaction (DOI) between the unburnt gas flow through the vent, creating turbulence, and the internal explosion. A few fitting parameters remain, tuned on existing experimental data. Since the number of data increased over time, various versions of this model were proposed (1999, 2001, 2008). The correlations and fitted parameters are given in the following tables.

Table 3 Correlations of 1999; 2001 and 2008 Molkov models

Bradley number	$Br = \frac{A_v}{V^{2/3}} \cdot \frac{c_u}{S_u(E-1)} \quad (9)$
Degree Of Interaction	$DOI = \alpha \left[\frac{(1 + eV_{\#}^g)(1 + 0.5Br^\beta)}{1 + P_v} \right]^\delta P_{i\#}^\omega \quad (10)$
Turbulent Bradley number	$Br_t = \frac{\sqrt{E/\gamma}}{\sqrt[3]{36\pi}} \frac{Br}{DOI} \quad (11)$
Reduced overpressure (1999)	$P_{red} = Br_t^{-2.4} \quad (if \ Br_t > 1; \ P_{red} < 1)$ $P_{red} = 7 - 6 * Br_t^{0.5} \quad (if \ Br_t < 1; \ P_{red} > 1) \quad (12)$
Reduced overpressure (2001)	$\frac{\pi_{red}}{\pi_v^{2.5}} = 5.65 * Br_t^{-2.5} \quad (If \ Br_t > 2; \ \frac{\pi_{red}}{\pi_v^{2.5}} < 1) \quad (13)$
Reduced overpressure (2008)	$\frac{\pi_{red}}{\pi_v^{2.5}} = 7.9 - 5.8 * Br_t^{0.25} \quad (If \ Br_t < 2; \ \frac{\pi_{red}}{\pi_v^{2.5}} > 1) \quad (14)$

These formulas rely on the definition of Degree of Interaction factor (DOI) which coefficients were initially determined empirically:

Table 4 Empirical coefficients for the DOI number correlation of 1999; 2001 and 2008 models

Model	α	B	δ	E	g	ω
1999	0.9	1	0.37	10	0.33	0
2001	1	0.8	0.4	10	0.33	0.6
2008	1	0.8	0.4	2	0.94	0

Where E is the combustion products expansion coefficient; γ the reactants specific heat ratio; A_v the vent area (m^2); V, the volume of enclosure (m^3); S_u , the initial laminar burning velocity (m/s); c_u the speed of sound (m/s); $V_{\#}$ the dimensionless volume (numerically equal to enclosure volume in cubic meters); P_v , the dimensionless static activation pressure ($P_v = (P_{stat} + P_i)/P_i$); $P_{i\#}$, the dimensionless initial pressure (numerically equal to initial pressure in absolute atmospheres); P_i the initial pressure (Pa) and P_{stat} the static activation pressure (Pa).

Later, Molkov et al. (2014) proposed a new way to estimate DOI based on the findings and methods used derived computational fluid dynamics (CFD) calculations. The DOI number was since then defined a product of flame wrinkling factors:

$$DOI = \Xi_K * \Xi_{LP} * \Xi_{FR} * \Xi_{u'} * \Xi_{AR} * \Xi_O \quad (15)$$

- Ξ_K is the wrinkling factor due the Landau-Darrieus flame instabilities.
- Ξ_{LP} is the wrinkling factor due to “leading point” mechanism, related to flame acceleration toward the vent.
- Ξ_{FR} is the wrinkling factor due to fractal increase of flame surface area linked to the development of the Rayleigh-Taylor instabilities.
- Ξ_{AR} a wrinkling factor to account for aspect ratio of the enclosure
- Ξ_O is the wrinkling factor to account for the presence of obstacles. Because of limited data, Molkov admitted that $\Xi_O = 1$ without obstacles and $\Xi_O = 3.5$ when obstacles are located between the ignition point and the vent.
- $\Xi_{u'}$ is the wrinkling factor due to the initial turbulence defined on the basis of the disturbed laminar burning velocity :

Along with this updated version of the DOI, the following new correlation estimate Pred was given:

$$P_{red} = 0.91 * Br_t^{-1.06} \quad (16)$$

Comparisons between these different models were made by Rocourt et al. (2013) and Jallais and Kudriakov (2013). It was concluded that the model of 1999 generally gave the best results as compared to that of 2001 and 2008. The latter version of the model (2014) was not available at that time.

4.3 FM Global Model (Bauwens, 2012)

Bauwens's model (2012) proposes an estimation of the major pressure peaks P identified in experiments (those described by Cooper et al., 1986). A single expression is used for all of those:

$$\frac{P_-}{P_0} = \frac{P_e}{P_0} \left(1 - \frac{\left(\frac{\gamma+1}{2}\right)^{\frac{\gamma}{\gamma-1}}}{(A_v^*)^2} \right)^{-1} \quad (17)$$

$$\text{with: } A_v^* = C_D \left(\frac{R T_v \gamma (\gamma+1)}{2 M_v} \right)^{\frac{1}{2}} \cdot \frac{a_{cd} A_v}{S_u A_f (\sigma-1)} \quad (18)$$

Where P₋, A_v, and A_v^{*} are pressure (for the different peaks), vent area, the "vent parameter" and the subscripts 0, e, f, and v corresponding to ambient, external, flame and vent conditions. In addition, E, γ, cd, R, T_v, and M_v are the expansion ratio, the specific heat ratio, a discharge coefficient (equal to 0.6), the universal gas constant (8.314 J/kg/mol), and the temperature and molar mass of the vented gas, respectively.

In case of an ignition on the wall opposed to the vent, the different values of P are estimated by choosing appropriate values for A_f and S_u; as shown in the table thereafter:

Table 5 A_f and S_u for the different values of P

Pressure peak (see Cooper 1986, Fig. 4)	A _f	S _u	Equations
P2	$A_{f(P1-BW)} \sim 2\pi \left[\frac{L^p h^p + L^p w^p + w^p h^p}{3} \right]^{\frac{1}{p}}$	$S_u \sim \frac{0.9}{Le} S_L$	(19)
P3	$\frac{A_{f\text{ obst}}}{A_f} = \left(1 + \frac{4}{3} \sigma^{1-\alpha} (BR)^{\frac{1}{2}} N^\alpha \right)^2$	$S_u \sim \frac{0.9}{Le} S_L$	(20)
P4	$A_{f(P2)} = 0.9 (A_{cw} - A_{contact})$ With $A_{contact} = 0.9 (A_{BW} - A_v)$	$S_u \sim \Xi_A S_L$	(21)

Where p = 1.6075, L, is twice the length of the enclosure; w the width and h height. A_{cw} is the internal area of the enclosure, α=0.63, BR is the average area blockage and N is the average number of layers of obstacles in the flame path. S_L is the laminar burning velocity and Le the Lewis number. Ξ_A is an empirically determined constant flame-wrinkling factor. Note that if the ignition does not occur on the face opposed to the vent, different formulas are proposed by Bauwens et al. (2012).

In terms of physics, this model is more accessible than that of Molkov. However, Jallais and Kudriakov (2013) showed that, in presence of obstacles, the results of the experiments of Daubech et al. (2013) are not correctly estimated (overestimation by at least a factor 2). Also, for small enclosures, the maximum internal overpressure of a vented deflagration tends to the maximum adiabatic overpressure (10 b) which is unrealistic.

4.4 INERIS's SECEX model

To model confined gas explosion phenomena and keep a satisfying understanding on the course of the events, INERIS developed the SECEX code, a phenomenological software consisting of interlinked models each dedicated to a single aspect such as flame propagation in a volume, turbulence characteristics prediction,

combustion rates, mechanical resistance, pressure effects... Deeper details on this model may be found in recent works of Proust and Leprette (2010), Daubech et al. (2016) and Duclos (2019). Most of the physics is derived from fundamental research. Each model is qualified separately, and the overall consistency can be compared to realistic full-scale experimentation or actual accidents. This tool has been designed in a context of process safety; this implies that it was built to provide conservative estimations in most situations. To model the secondary explosion phenomenon the model partly relies on empirical observations. In the vessel, the flame is modelled as an ellipsoid surface directed towards the vent. In front of the vent, Lannoy (1984) model is used to estimate the overpressure effects of the secondary explosions:

$$\Delta P_{ext} = \frac{3}{2} \cdot \rho \cdot V_{exp}^2 \quad (22)$$

with V_{exp} , the flame velocity in front of the vent. V_{exp} was measured in INERIS tests and an empirical correlation (Proust and Leprette, 2010) was extracted from these tests to determine a value of V_{exp} for the other tests of the database (Figure 5).

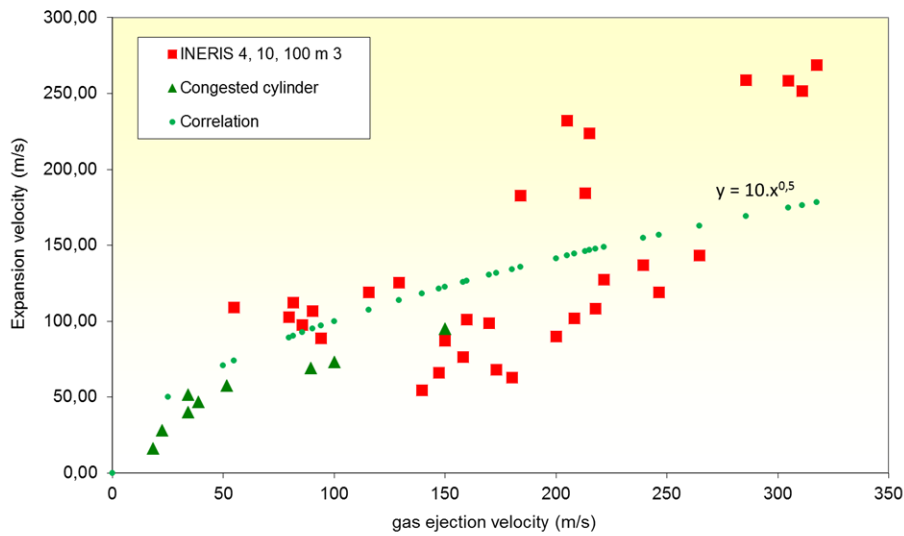


Fig. 5. Proust et Leprette (2010) correlation on the outer cloud expansion velocity during vented gas explosions

The correlation takes the form:

$$V_{exp} = 10 \cdot V_{vent}^{0,5} \quad (23)$$

The secondary explosion contribution to the internal pressure effects is considered under 2 angles: a part of the energy (proportional to the vent area over enclosure cross section ratio) contributes to the vessel compression while the overpressure outside also impedes the gas discharge through the vent. In terms of complexity this model is relatively simple as it does not need for instance, the knowledge of a flame wrinkling factor but it still relies on an iterative calculation and does not account for specific features such as obstacles.

The SECEX model yields the following results when applied to a part of the dataset (Duclos, 2019):

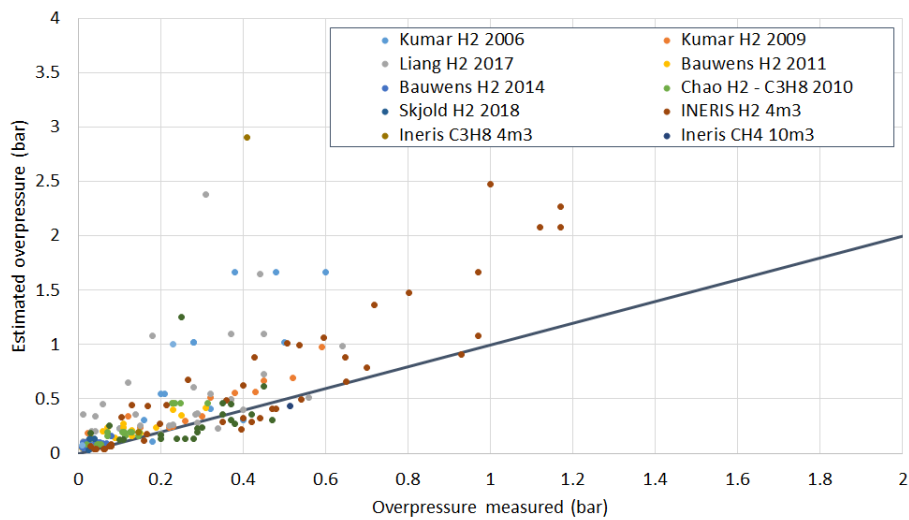


Fig. 6. Comparison of the SECEX tool estimations with experimental data.

The average absolute error is 245 mbar and the standard deviation 250 mbar on this set. Here we purposely showed a limited part of the dataset, consisting in tests performed in vessels of parallelepipedal shapes with vents of low P_{stat} , with is the reference configuration for which this model has been developed. The database mostly consists in test in this configuration but also includes cylindrical and spherical vessels and some tests with vent panels having a P_{stat} up to 300 mbar. Thus, on the full dataset the average error is bigger, on the order of 400 mbar.

4.5 Synthesis on the “traditional” modelling approach

Different limits are exposed for these models that have been design with different goals (pure vent dimensioning on a process, accurate estimation of the pressure peaks, description of secondary explosions, etc.). The accuracy of the prediction put aside, one can notice a certain complexity of each model which rely on highly non-linear equations, and in some cases: input parameters that may be difficult to access such as the wrinkling factor, the DOI or a specific flame surface calculation In contrast the neural network implementation does not require the user to solve equations and the input data here is chosen to be fairly easily accessible as it mostly consists in geometric dimensions of the experiment and information on the vent P_{stat} and the test conditions (gas nature, concentration, ignition location and initial turbulence).

5 Results of the ANN predictions

Results are presented for each of the cases described in the paragraph 3.

5.1 Basic configurations: general random data separation

In a first attempt, 10 % of the lines in the database are randomly selected and isolated as the test data (Table 6). The rest of the data – 268 – 26 = 242 test is augmented 100 times to build a 24442 lines matrix (242+242*100). It is used to train the neural network. Thus, the samples from the test database are different but should remain generally close to the training dataset. The typical results obtained in this configuration are shown in Fig. 7.

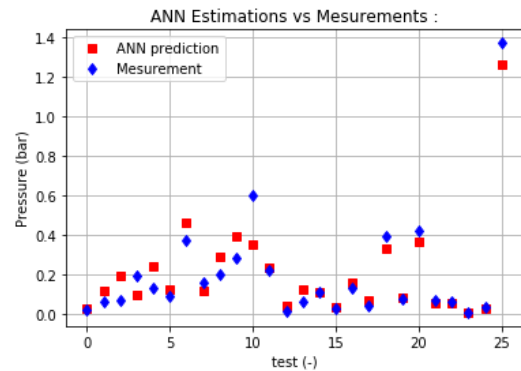
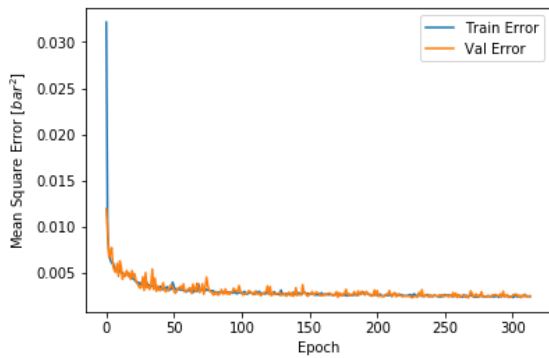


Fig. 7. a) typical convergence curves for the MLP training. b) comparison of ANN predictions and measurements on 26 randomly selected tests (not present in the training data)

The absolute error is 55 mbar (the average error is 6.2 mbar) and the standard deviation is also 55 mbar. If compared to the phenomenological model results, absolute error attained with the ANN is the lowest in 22 of the 26 cases, the latter showing an average error above 250 mbar. However, the ANN only leads to a conservative estimation in 16 cases versus 22 for the phenomenological model.

Among those randomly selected tests, only half (13) are sufficiently documented to compute the P_{red} with all the other models listed in section 4. In Fig. 8 (numerical data in table 7), the predictions obtained with the various models are presented. Those consist in tests with hydrogen, in the following test configurations:

Table 6 List of randomly selected tests in the database to verify the functioning of the neural network and for which sufficient data is available to estimate the overpressure with the models of NFPA68:2013, Bauwens et al. (2012) and Molkov et al. (1999, 2014). "I" refers to the ignition point: it is 0.5 if the ignition occurs in the center of the enclosure and 1 if it is carried out at the bottom opposite the vent. S.I units

Test	Author	Year	%vol	I	L	D	V	Av	u'	Su	E
A	Bauwens	2011	14.9	0.5	4.6	3,63	63.7	5.4	0.1	0.83	4.6
B	Bauwens	2011	18.1	0.5	4.6	3,63	63.7	5.4	0.1	1.3	5.2
C	Bauwens	2011	19	0.5	4.6	3,63	63.7	5.4	0.1	1.4	5.4
D	Bauwens	2011	18.3	1	4.6	3,63	63.7	5.4	0.1	1.32	5.25
E	Bauwens	2011	19	1	4.6	3,63	63.7	5.4	0.1	1.4	5.4
F	Bauwens	2011	15.1	1	4.6	3,63	63.7	2.7	0.1	0.85	4.6
G	Bauwens	2011	18.3	0.5	4.6	3,63	63.7	5.4	0.1	1.3	5.2
H	Bauwens	2011	18.5	0.5	4.6	3,63	63.7	5.4	0.1	1.35	5.3
I	Daubech	2011	27	1	1.66	0.94	1	0.13	0	2.5	6.6
J	Kumar	2006	11	1	10	3.43	120	0.55	0	0.36	3.65
K	Kumar	2009	10.2	0.5	10	3.43	120	0.55	1	0.27	3.42
L	Kumar	2009	8.8	0.5	10	3.43	120	1.1	1	0.19	3.1
M	Duclos	2019	16	1	2	1.33	4	0.49	0	1	4.8

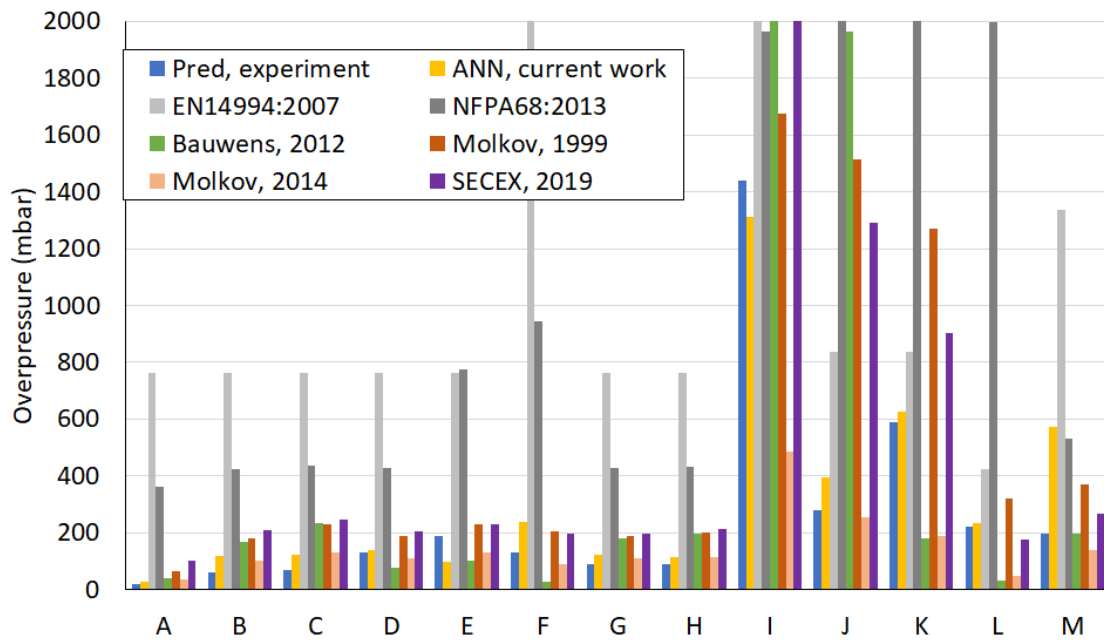


Fig. 8. Experimental measurement and results of predictions or calculations for the tests listed in **Table 6**

Table 7 Experimental measurement for the tests listed in **Table 6** and results of predictions using various models. Overpressures in mbar; ANN = Artificial Neural Network. The conservative best estimate is in *italic* and highlighted in green. Underestimates of effects are in **bold**, highlighted in red and dark red and underlined for strong underestimates of effects (greater than 100 mbar difference¹). M.A.E. stands for the mean absolute error (with respect to the experimental value, for each column here)

TEST	P _{red}	ANN	EN14994 2007	NFPA68 2013	Bauwens, 2012s	Molkov, 1999	Molkov, 2014	SECEX, 2019
A	20	<i>30</i>	765	365	40	65	35	100
B	60	<i>120</i>	765	425	170	180	<i>100</i>	210
C	70	<i>120</i>	765	440	235	230	135	245
D	130	<i>140</i>	765	425	80	190	110	205
E	190	95	765	775	100	<i>230</i>	135	<i>230</i>
F	130	240	2510	945	<u>30</u>	205	90	<i>200</i>
G	90	125	765	425	180	190	<i>110</i>	200
H	90	<i>115</i>	765	430	195	200	<i>115</i>	215
I	1440	1310	3970	1965	3265	<i>1675</i>	<u>485</u>	5455
J	280	<i>395</i>	835	5850	1965	1515	255	1290
K	590	<i>630</i>	835	5135	<u>180</u>	1270	<u>190</u>	905
L	220	<i>235</i>	420	1995	<u>30</u>	320	<u>45</u>	175
M	195	575	1335	535	<i>195</i>	370	140	270
M.A.E.	-	85	905	1245	370	240	145	485

¹ see details in the article for explanations on this threshold

These results point out an overall better efficiency of the neural network. Worse, if only the mean absolute error is retained (which is certainly not a good practice if industrial safety is considered), this model performs at least about twice better than any other, on this specific sample. Of course, a statistical analysis on such small sample is irrelevant. Furthermore, it has been chosen to highlight the best result at each line of **Table 7**, not considering that in some cases other models also lead to very satisfying estimations, which is disputable, considering that a 20 mbar difference is negligible on such measurements. The discrimination between lower and stronger (above 100 mbar) underestimates remains also subjective. In comparison, one can put on the line that the 100 mbar values correspond to the static opening pressure of most explosion vents and the lower limit for the Pstat parameter in the European standard vent dimensioning formulas. The objective here is to give a focus on the excellent performance of the neural network, on these tests that were chosen randomly in the database, given the fact that barely any time was spent by the authors studying the physics or configuring the neural network, as we basically kept the example proposed on the official website of TensorFlow. Furthermore, the computation cost is negligible at this scale, as a few minutes are needed on a standard CPU to train the neural network while the prediction phase is practically instantaneous.

However, if the ANN model can be seen as some sort of polynomial fit over the dataset, one can expect that close configurations will yield results close to those used for the regression as effectively shown here. The real problem is in the generalisation capabilities of the model.

5.2 Laboratory/Group data separation

The data is split in 2 sets: one contains all the tests performed at INERIS (105 tests), the other contains the measurements published by other researchers (163 tests). In one case INERIS data is used to train the ANN and the other set is the test data. In the second case it is the opposite. This illustrative path yields the following results:

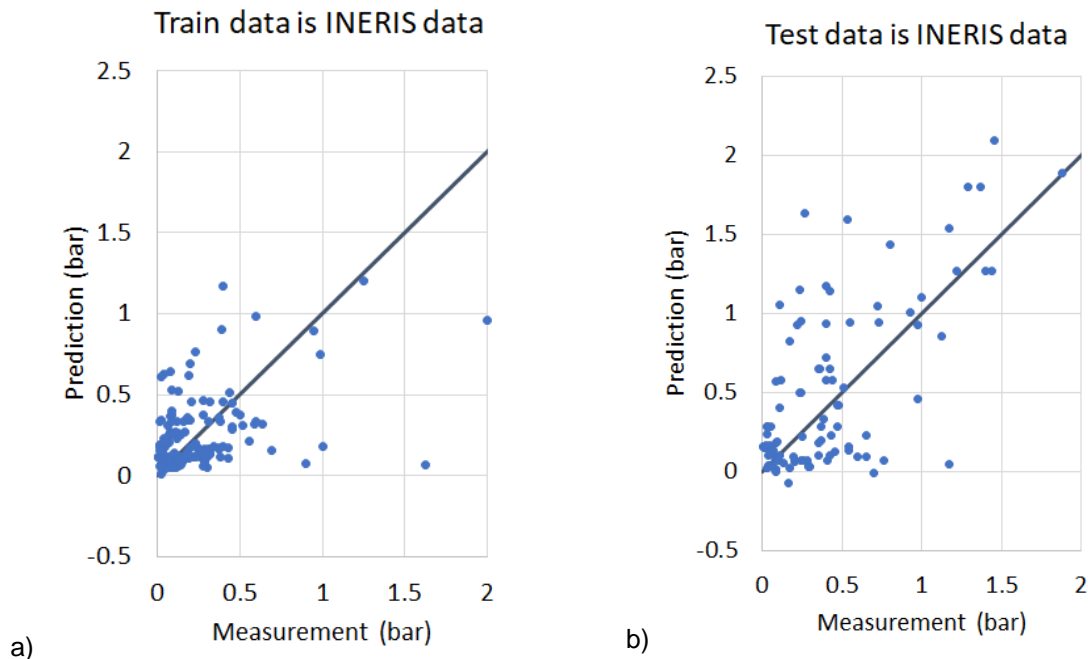


Fig. 9. ANN Predictions vs. measurements for datasets arranged by laboratory: a) the train data is that of INERIS while the test data is the other published test and b) opposite case: the train data is the published test from other laboratories while INERIS data is the test data.

It seems that INERIS dataset is slightly better to train the ANN. In some occurrences unphysical results such as negative overpressures may be found. However, in both cases large discrepancies appear, confirming that the missing data has an adverse effect on the neural network performance.

Another test was run selecting randomly 3 groups of data as test data (and removed from the initial database used to train the neural network). As a reminder, we define as a “group of data”, the tests performed by a same author, during a same study with a single combustible gas and a single volume. The operation has been repeated 3 times (i.e. 3 random selections of 3 groups), leading to a total of 89 tests, to limit the bias introduced by the random selection of the samples. An histogram classifying the relative differences between the predictions / estimations (respectively of the ANN and the SECEX tool) and the experimental measurements are presented in **Fig. 10.**:

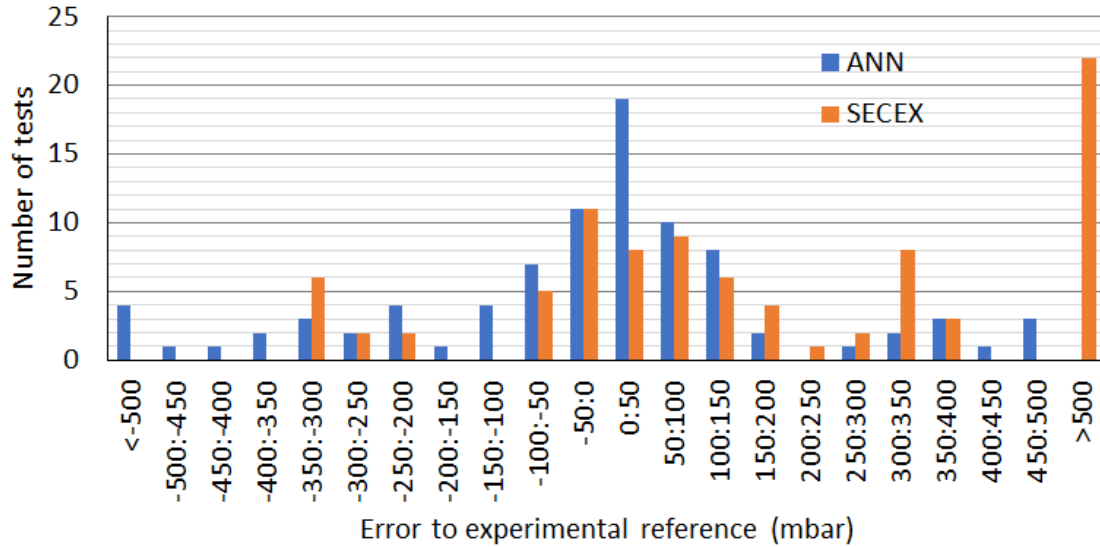


Fig. 10. Histogram of the relative error (prediction/estimation minus experimental measurement) calculated with the ANN and the SECEX models when randomly selecting as test data 3 studies in the initial dataset (again those are not used in the training phase and the graphic is compilation of the results of 3 trained neural networks).

So, this appear that despite it needs to rely on significant amount of data, the ANN approach yields consistent results and can often provide estimations that are on average closer to the experimental measurement than those given by the physics-based code. However, the errors are evenly distributed around zero, while with the SECEX model, most of the estimations yield conservative results. Such result was expected as the ANN was designed to fit data while the SECEX model is set to provide conservative estimations, so that it could be use in a context of industrial safety. It is however conceivable to tweak a neural network to reproduce such behaviour, for example by purposely increasing the targeted pressures values by a few percent in the training phase or applying safety margins on the network output.

5.3 Physical relevancy

In this section, the interest is focused on the behaviour of the ANN model. A sort of “sensitivity analysis” is performed to evaluate the physical relevancy of the model proposed by the neural network. In practice, the ANN is firstly trained with the whole dataset. Then 2 representative test configurations are selected in the database for which the largest amount of “resembling” data is available. The objective is to have the largest confidence in the capabilities of the neural network in the vicinity of those 2 configurations (Table 8).

Table 8 Reference configurations selected for the physics tests

Comb.	%Vol	Length (m)	Diameter (m)	Volume (m ³)	Ignition	Vent area (m ²)	Pstat (bar)	u' (m/s)
H ₂	19	4.6	3.63	63.7	Central	5.4	0.005	0.1
CH ₄	10	4.6	3.63	63.7	Central	5.4	0.005	0.1

From these 2 test configurations, test data is produced by varying a single input parameter (for instance the gas concentration) and keeping the other parameters constants. In the current examples, the varied parameters are:

- the volume % of the combustible gas in air, which is varied from 0 to 80 %,
- the vent area, which is varied from 1 to 25 m²,
- the vent P_{stat}, which is varied between 5 and 200 mbar.

First, for the volume concentration, the code leads to the results presented in figure 11. Clearly meaningless results are produced with negative overpressures.

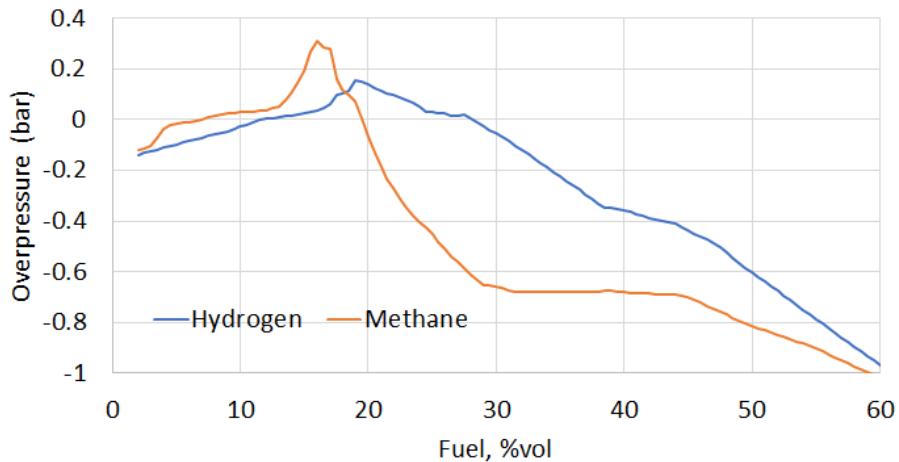


Fig. 11. ANN predictions as function of fuel fraction in air

Note that for methane, the tests were performed in the 8-13 % range with a large majority of tests around 10 %, while those with hydrogen in the 5-34 % range, with a large majority of tests around 20 %. As already known, the ANN entirely ignores the physics, but it is especially critical here for the hydrogen case. Indeed, the model even fails to yield physical result in the when the gas concentration exceeds 28 %. Note that one could have expected a better performance as the database includes tests with volume fraction up to 34 % (yet not on this 63.7 m³ vessel). In the methane case, negative overpressures are reached after 20% but it is not as critical as in the hydrogen case: the higher explosive limit of methane being located around 15%, the mixture is not explosive and this result is less prone to dramatic misinterpretations. A slight improvement of the model could be made assuming that the overpressure is null as soon as the gas mixture is out of the explosivity range of the gases (about 5-15% for methane in air and 4-75% for hydrogen).

Those curves are globally showing false trends, if the whole picture is examined. However, they should be also presenting physically representative trends in a local window more representative of the training dataset. Unfortunately, the discrimination between both behaviours is difficult. A better mastering of the neural network, and in particular a way to constrain it to respect specific physical laws such as the “P_{red} is higher than P_{stat}” may be helpful to verify trends or derive new empirical models from these predictions. Such approach seems possible working on the ANN loss function and output conditions (Liu et Wang, 2019), but it involves significant effort and a deeper understanding in neural network processing.

Because the initialisation of the network is based on initial random numbers and the training consists in minimizing the error of a group of functions, the neural network, despite leading to similar results within its functioning range, is never the same after a training phase. Thus, a solution to the problem of the definition of the range of validity of the ANN could be to train a second network (that may keep the same architecture, to save possible computational development costs) on the exact same training dataset. Doing so, when the same test data is introduced in this a second version of our ANN, named v2 we obtain the curves of **Fig. 12**. The prediction may not be more relevant but now the regions where V1 and V2 diverge are likely to point out the ranges where the ANN method fails.

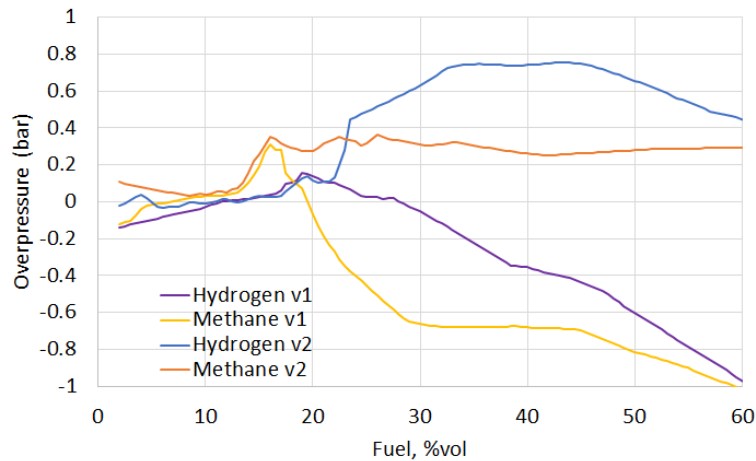


Fig. 12. ANN predictions as function of fuel fraction in air. Comparison of 2 versions of the ANN

Alternatively, a good superposition enhances but does not guarantees good predictions. Because of the low computational costs involved in such approach, it could be extended to larger numbers of iterations. Note that for the methane case the 2 MLP lead to similar result over most of the flammability range (8-13% to compare to 5-15%), indicating that on this specific configuration (cylindrical vessel of volume 63.7 m³ with a 5.4 m² vent and a P_{stat} as low as 5 mbar) the amount of training data could be dense enough to perform reliable estimations. Further tests remain needed to validate or extend this hypothesis.

In the following, two versions of the ANN are systematically employed. Note that this method may be insufficient to trace out of all the validity difficulties. Again, the objective of current paper is to provide information on the practice rather than an efficient model.

The effect of vent area and vent bursting pressure is shown on **Fig. 13**:

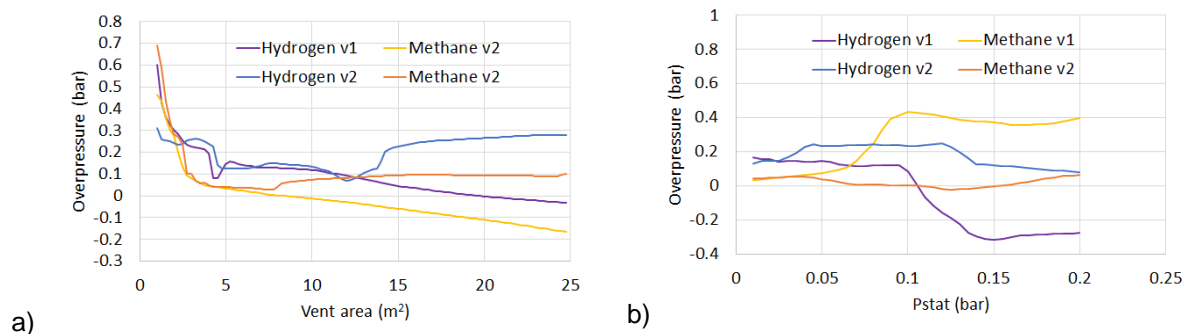


Fig. 13. ANN predictions as function of vent area (a) or vent P_{stat} (b)

Concerning the vent area, for methane the ANN clearly indicates a strong influence on P_{red} decreasing for vent sizes increasing from 1 to 6 m². This is an expected physical behaviour. In further details it appears that in this area the vent size is linearly dependent on the square root of the overpressure, with is in line with the “traditional” models for vent dimensioning shown in paragraph 4. Thus, using neural networks in such way could also be useful to develop new physical models. The agreement is not as good for the case of hydrogen and vent areas around 3-4 m² but the overall trend is still respected.

However, the agreement is generally poor on the vents P_{stat}. On the initial training dataset, most of the tests are performed with vents of P_{stat} lower than 20 mbar (200 over 268 tests), often assumed to be close to 5 mbar, in the absence of any better measurement (as said earlier, these vents often consisted in plastic foils glued or taped on the vessels). In any case, this underlines the strong dependency of the network estimations on consistency of the dataset used to train it.

5.4 Robustness

Other tests of this kind, on the vessel volume or turbulence intensity could be made, but it is not the object of current paper. The authors wish to point out the specific difficulty that may be encountered when dealing with these algorithms and linked to their extreme robustness. The exercise performed in section 5.1 in which 10% of the dataset is selected as test data is conducted a second time with the exact same tests (no new random selection), but with the introduction of an error in the training dataset. It consists in shifting by 1 cell all the overpressures in the initial table (i.e. the last column of **Table 2**), the first value of the table is replaced arbitrarily by the last one. Note that this accidental shifting of the ANN output column could be due a manipulation error from the user such as a coding error in the table indexes. Then the data is augmented (see paragraph 3.5) and the ANN is trained with this corrupted dataset. The code yields the following results:

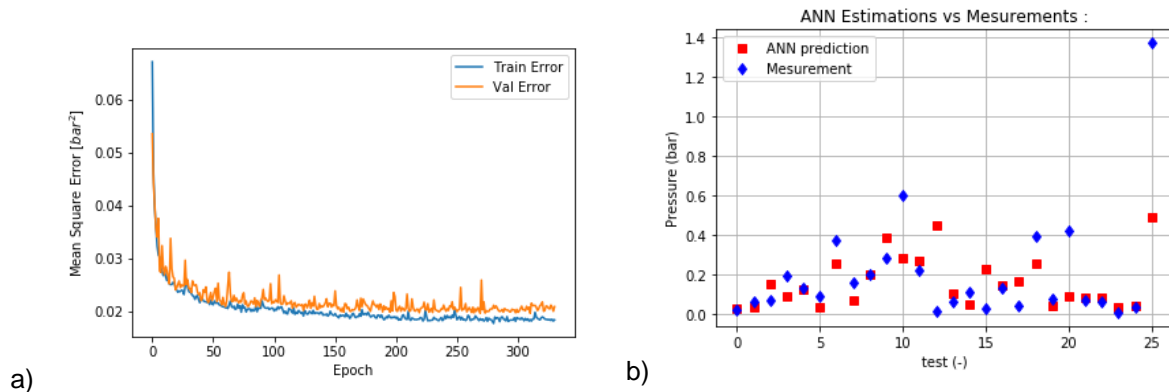


Fig. 14. a) Convergence curves for the ANN training with corrupted data. b) comparison of ANN predictions and measurements on the same 26 tests as in Fig.5 with the wrongly trained ANN.

Only limited differences appear between this case and that shown in Fig. 5. The absolute error is 125 mbar (versus 55 mbar before) and the standard deviation is 190 mbar (versus 55 mbar in Fig. 5.). In practice, there is no way to detect the error in the dataset: the ANN was trained on corrupted data on which it managed to perform an excellent fit. The output result is however subject to more randomness despite it is barely visible in the current case. Thus, because of their extreme ability to fit data, those algorithms, when they are trained with corrupted data, produce false models without the user being informed.

6 Discussion

On a general basis, in this work, a remarkable efficiency and robustness of the ANN based tool is shown, and in particular its extreme capability to fit data. As they stand, this kind of tools produces results based on a purely “inductive” method (Escande et al., 2013). Despite they consist in purely mathematic tools, with no physics behind, it is possible to extract general physical trends from the results. Note that in the current work, a single neural network architecture was selected and not modified for the whole study. It is based on the default pre-programmed parameters and online recommendations of the official TensorFlow’s tutorials. This underlines the simplicity of the task and the consequent work achieved by the developers of the concerned libraries. Placing more attention on the specific aspect of the network architecture could lead to an even increased performance of the tool described in the current paper. However, it is also show here that, despite its simplicity of implementation, this type of calculation is far from trivial and the results of simulations made with this type of model must be examined with the greatest care. If the code is intended to be empirical, the critical analysis of the results may nonetheless be very complex because of:

- the data: the multiplicity of hypotheses that can be made on the training data is a first complexity if for example, as here, we rely on data from very different sources, more or less documented. Note that the selection of the meaning parameters covering the phenomenology (ex: if nature of the gas is lacking a relevant parameter would lack) to include in the data is a critical part of the physicist job in this problem – the other part being the examination of the results consistency in regard to physics law’s (for instance obtaining positive pressures at the outputs of the ANN). Having a significant amount

of data is critical to build the model, which may pose a difficulty as real scale explosion tests are expensive. A numerical data augmentation method based on the measurement's accuracy was proposed and successfully tested, but it can be seen as a way to weight certain selected tests and to orientate the ANN. This may not be satisfactory.

- *the structure of the network*: there is a great diversity of possible neural architectures: we did not focus on this point because it was not the object of the study, but the construction of the network is based on choices on the number of neurons, of layers of neurons, of minimization criteria, of convergence, a certain number of iterations or of output parameters. An interesting alternative solution would consist in the adding physical constraints. In addition of releasing the limitation of the breadth of the database, this solution may help to avoid the well-known intrinsic limitations of “inductive” method. “Physically” guided neural network exist and have been the object of publications in various fields (for example refer to Liu et Wang, 2019). In the present example, it could consist for instance in specifying that in the absence of the vent, the P_{red} obtained is the gas P_{max} or that at too lean or to rich concentrations, the P_{red} is 0.
- *the choice of the outputs*: one chose the P_{red} here but one could have asked as well the 4 peaks of pressure of Cooper's model (1986), a signal of pressure or a physical parameter like a term of speed of flame to be used then in other models. In the meantime, it is suggested to perform comparison of several models trained on the same datasets, to verify locally the overall consistency of the model predictions. Two models trained on the same data should lead to similar predictions. When it is not the case, it may mean that the ANN perform an extrapolation too far from the initial training dataset.

Finally, it is envisioned that once enough confidence on the ANN is reached, a parametric study on its input data is a computationally cheap way to extract or verify empirical observations as well as developing new physical models. It may for instance be useful to identify specific behaviours, unknown sensitive variables or unknown unknowns in a problem.

7 Conclusions

The problem of overpressure generated during a gas explosion in a vented enclosure has been examined under the angle of a regression problem with the use of a multilayer perceptron, a specific type of artificial neural network. The use of such algorithms drastically increased over the past 5 year and is particularly supported by the publication from a few sector leaders of open source tools such as TensorFlow, among others. These tools were specifically designed in view of simplifying and democratizing the access to neural networks and the associated methods. In the current work, a remarkable efficiency and robustness of such tools is shown, and in particular their extreme capability to fit data. However, it is also demonstrated that despite its simplicity of implementation, this type of calculation is far from trivial and the results of simulations made with this type of model must be examined with the greatest care. Recommendations are made, mostly on the training data and the necessary post-processing of the results in view of improving the interpretability of the results obtained with such method.

8 References

Abadi, M., Agarwal, A., Barham, P., Brevdo, E., Chen, Z., Citro, C., Corrado, G.S., Davis, A., Dean, J., Devin, M., Ghemawat, S., Goodfellow, I., Harp, A., Irving, G., Isard, M., Jia, Y., Jozefowicz, R., Kaiser, L., Kudlur, M., Levenberg, J., Mane, D., Monga, R., Moore, S., Murray, D., Olah, C., Schuster, M., Shlens, J., Steiner, B., Sutskever, I., Talwar, K., Tucker, P., Vanhoucke, V., Vasudevan, V., Viegas, F., Vinyals, O., Warden, P., Wattenberg, M., Wicke, M., Yu, Y., Zheng, X., 2016. TensorFlow: Large-Scale Machine Learning on Heterogeneous Distributed Systems.

Bauwens, C.R., Chaffee, J., Dorofeev, S.B., 2011. Vented explosion overpressures from combustion of hydrogen and hydrocarbon mixtures. *International Journal of Hydrogen Energy* 36, 2329–2336. <https://doi.org/10.1016/j.ijhydene.2010.04.005>

- Bauwens, C.R., Chao, J., Dorofeev, S.B., 2012a. Effect of hydrogen concentration on vented explosion overpressures from lean hydrogen–air deflagrations. *International Journal of Hydrogen Energy* 37, 17599–17605. <https://doi.org/10.1016/j.ijhydene.2012.04.053>
- Bauwens, C.R., Chao, J., and Dorofeev, S. B., 2012b, Evaluation of a multi peak explosion vent sizing methodology, IX ISHPMIE. International Symposium on Hazard, Prevention and Mitigation of Industrial Explosions
- Bauwens, C.R., Dorofeev, S.B., 2014. Effect of initial turbulence on vented explosion overpressures from lean hydrogen–air deflagrations. *International Journal of Hydrogen Energy* 39, 20509–20515. <https://doi.org/10.1016/j.ijhydene.2014.04.118>
- Chao, J., Bauwens, C.R., Dorofeev, S.B., 2011. An analysis of peak overpressures in vented gaseous explosions. *Proceedings of the Combustion Institute* 33, 2367–2374. <https://doi.org/10.1016/j.proci.2010.06.144>
- Chollet, F., and others., 2015, Keras. <https://keras.io>.
- Cybenko, G. 1989. Approximation by superpositions of a sigmoidal function *Mathematics of Control, Signals, and Systems*, 2(4), 303–314.
- Daubech J., Proust C., Jamois D., Leprette E., 2011, Dynamics of vented hydrogen-air deflagrations, *Proceedings of the 4th International Conference on Hydrogen Safety (ICHHS)*, Sep 2011, San Francisco, United States. ineris-00973626f, <https://hal-ineris.archives-ouvertes.fr/ineris-00973626/document>
- Daubech J., Proust C. and Lecocq G., 2016, Propagation of a confined explosion to an external cloud, 11th International Symposium on Hazards, Prevention and Mitigation of Industrial Explosions, Dalian, China
- Demsar J, Curk T, Erjavec A, Gorup C, Hocevar T, Milutinovic M, Mozina M, Polajnar M, Toplak M, Staric A, Stajdohar M, Umek L, Zagar L, Zbontar J, Zitnik M, Zupan B, 2013, Orange: Data Mining Toolbox in Python, *Journal of Machine Learning Research* 14(Aug): 2349–2353
- Duclos A., 2019, Développement de modèles phénoménologiques et de maîtrise des risques d'explosion pour la filière émergente hydrogène-énergie. Manuscrit de thèse. Université de Technologie de Compiègne
- Escande J., Le Coze J.-C., Proust C., Marlair G., 2013 Signaux faibles : un concept pertinent ?. 14. Congrès de la Société Française de Génie des Procédés "Les sciences du génie des procédés pour une industrie durable" (SFGP 2013), Oct 2013, Lyon, France. pp.NC. ineris-00973715
- Fakandu, B.M., Yan, Z.X., Phylaktou, H.N., Andrews, G.E., 2013. The Effect of Vent Area Distribution in Gas Explosion Venting and Turbulent Length Scale Influence on the External Explosion Overpressure, *Proceedings of the Seventh International Seminar Fire and Explosion Hazards*. Research Publishing Services, pp. 717–726. https://doi.org/10.3850/978-981-07-5936-0_11-05
- Grégoire, Y., 2021 Vented gas explosion overpressure calculation based on a multi-layered neural network - Code and data. In journal of loss prevention in the process industries (Version 1). Zenodo. <https://doi.org/10.5281/zenodo.5497942>
- Jallais S., Kudriakov S. An inter-comparison exercise on engineering models capabilities to simulate hydrogen vented explosions, ICHS5; Brussels September 2013 Paper 176
- Karpathy A., 2015, The Unreasonable Effectiveness of Recurrent Neural Networks, Hacker's guide to Neural Andrej Karpathy blog, <https://karpathy.github.io/2015/05/21/rnn-effectiveness/>
- Kumar, R.K., Dewit, W.A., Greig, D.R., 1989. Vented Explosion of Hydrogen-Air Mixtures in a Large Volume. *Combustion Science and Technology* 66, 251–266. <https://doi.org/10.1080/00102208908947153>
- Kumar, K., 2006. Vented Combustion Of Hydrogen-Air Mixtures In A Large Rectangular Volume, in: 44th AIAA Aerospace Sciences Meeting and Exhibit. Presented at the 44th AIAA Aerospace Sciences Meeting and Exhibit, American Institute of Aeronautics and Astronautics, Reno, Nevada. <https://doi.org/10.2514/6.2006-375>
- Kumar, R. K., 2009, Vented Turbulent Combustion of Hydrogen-Air Mixtures in A Large Rectangular Volume. In 47th AIAA aerospace sciences meeting including the new horizons forum and aerospace exposition. Paper AIAA 2009-1380
- Lannoy A., 1984, Analyse des explosions air-hydrocarbure en milieu libre : Etudes déterministe et probabiliste du scénario d'accident. Prévision des effets de suppression. Bulletin Direct. Etudes et Recherches EDF. A4

- Liang, Z., 2017. Scaling effects of vented deflagrations for near lean flammability limit hydrogen-air mixtures in large scale rectangular volumes. *International Journal of Hydrogen Energy* 42, 7089–7103. <https://doi.org/10.1016/j.ijhydene.2016.12.086>
- Liu, D., Wang, Y., 2019. Multi-Fidelity Physics-Constrained Neural Network and Its Application in Materials Modeling. *Journal of Mechanical Design* 141, 121403. <https://doi.org/10.1115/1.4044400>
- Molkov, V., Dobashi, R., Suzuki, M., Hirano, T., 1999. Modeling of vented hydrogen-air deflagrations and correlations for vent sizing. *J. Loss Prev. Process. Ind.* 12, 147–156. [https://doi.org/10.1016/S0950-4230\(98\)00049-7](https://doi.org/10.1016/S0950-4230(98)00049-7).
- Molkov, V., Shentsov, V., Quintiere, J., 2014. Passive ventilation of a sustained gaseous release in an enclosure with one vent. *Int. J. Hydrogen Energy* 39 (15), 8158–8168.
- Pasman, H.J., Groothuisen, Th.M. and Gooijer, P.H., 1974, Design of Pressure Relief Vents, In *Loss Prevention and Safety Promotion in the Process Industries*, Ed. Buschman C.H., New-York, 185-189.
- Proust, C. and Leprette, E., 2010, The dynamics of vented gas explosions, *Process Safety Progress*, vol. 29, 3, 2010, pp. 231–235
- Rocourt X., Awamat S., Sochet I., Jallais S. Vented hydrogen-air deflagrations in a small enclosed volume, ICHS5; Brussels September 2013 Paper 135
- Rodgers et Zalosh, 2013, NFPA 68 new gas venting equations, *Proceedings of the 9th Global Congress on Process Safety*, 28 April - 2 May 2013, San Antonio, Texas, USA
- Skjold, T., Hisken, H., Lakshmipathy, S., Atanga, G., Bernard, L., van Wingerden, M., Olsen, K.L., Holme, M.N., Turøy, N.M., Mykleby, M., van Wingerden, K., 2019. Vented hydrogen deflagrations in containers: Effect of congestion for homogeneous and inhomogeneous mixtures. *International Journal of Hydrogen Energy* 44, 8819–8832. <https://doi.org/10.1016/j.ijhydene.2018.10.010>
- Sun, S., Wang, M., Gao, K., Zhao, T., Guo, Q., 2018. Effect of vent conditions on internal overpressure time-history during a vented explosion. *Journal of Loss Prevention in the Process Industries* 54, 85–92. <https://doi.org/10.1016/j.jlp.2018.03.002>
- Wang, J., Guo, J., Yang, F., Zhang, J., Lu, S., 2018. Effects of hydrogen concentration on the vented deflagration of hydrogen-air mixtures in a 1-m³ vessel. *International Journal of Hydrogen Energy* 43, 21161–21168. <https://doi.org/10.1016/j.ijhydene.2018.09.108>
- Yao C., 1974, Explosion venting of low strength equipment and structures. *AIChE Loss Prevention Symposium*, Vol. 8